Atmos. Chem. Phys. Discuss., 12, 13053–13087, 2012
www.atmos-chem-phys-discuss.net/12/13053/2012/
doi:10.5194/acpd-12-13053-2012

Atmospheric Chemistry and Physics Discussions

Mid-tropospheric δD observations from IASI/MetOp at high spatial and temporal resolution

J.-L. Lacour[1], C. Risi[2], L. Clarisse[1], S. Bony[2], D. Hurtmans[1], C. Clerbaux[3,1], and P.-F. Coheur[1]

[1]Spectroscopie de l'Atmosphère, Service de Chimie Quantique et Photophysique, Université Libre de Bruxelles, Belgium
[2]LMD/IPSL, CNRS, Paris, France
[3]UPMC Univ. Paris 06; Université Versailles St.-Quentin; CNRS/INSU, LATMOS-IPSL, Paris, France

Received: 18 April 2012 – Accepted: 10 May 2012 – Published: 25 May 2012

Correspondence to: J.-L. Lacour (jlacour@ulb.ac.be)

Published by Copernicus Publications on behalf of the European Geosciences Union.

Abstract

In this paper we present a method to retrieve HDO, H_2O and δD from IASI radiances spectra. It relies on an existing radiative transfer model (Atmosphit) and optimal estimation inversion scheme, but goes further than our previous work by explicitly considering correlations between the two species. Global (fixed) HDO and H_2O a priori profiles together with a covariance matrix were built from daily model simulations of HDO and H_2O profiles (the LMDz-iso model is used) over the whole globe and a whole year. The retrieval parameters are described and characterized in terms of errors. We show that IASI is mostly sensitive to δD in the middle troposphere and allows retrieving δD for an integrated 3–6 km column with an error of 38 ‰ on an individual measurement basis. We examine the performance of the retrieval to capture the temporal (seasonal and short-term) and spatial variations of δD by analyzing one year of measurement at two dedicated sites (Darwin and Izaña) and a latitudinal band from −60° to 60° for a 15 days period in January. The performances are compared with LMDz-iso simulations. We report a general excellent agreement between IASI and the model and demonstrate the capabilities of IASI to reproduce the large scale variations of δD (seasonal cycle and latitudinal gradient) with good accuracy. In particular, we show that there is no systematic significant bias in the retrieved δD values in comparison with the model, and that the retrieved variability is similar to the modeled one although there are certain significant differences depending on the location. Moreover the noticeable differences between IASI and the model reported and briefly examined tend to suggest modeling issues instead of retrieval effects. Finally, we strengthen the unprecedented capabilities of IASI to capture short-term variations in δD, further highlighting the added value of the sounder for monitoring hydrological processes.

ACPD
12, 13053–13087, 2012

1 Introduction

Water vapor is a key gas for the climate system. Its radiative properties make it the strongest infrared absorbing gas of our atmosphere, contributing to approximately 50 % of the total greenhouse effect (Schmidt et al., 2010; Kiehl and Trenberth, 1997). Moist processes also play a key role in controlling the large-scale atmospheric circulation (Randall et al., 1989; Frierson, 2007) and its sensitivity to climate forcing (Kang et al., 2008; Zhang et al., 2010). Even though hydrological processes have been abundantly studied, there is still an insufficient understanding of the factors controlling water amount (Sherwood et al., 2010; Schneider et al., 2010b). As major climate feedbacks (cloud and water vapor feedbacks) are associated with tropospheric water vapor (Soden and Held, 2006; Bony et al., 2006), there is a need to better assess the mechanisms that control the humidity distribution in the troposphere.

Because vapor pressure depends on the mass of the water molecules, there is a fractionation of the different isotopologues during evaporation and condensation processes: heavier isotopologues ($H_2^{18}O$, $H_2^{17}O$ and HDO) have a saturation pressure and will preferentially condensate leading to a depletion of the heavier isotopologues. The isotopic composition of an air parcel therefore gives a fingerprint of the history of the phase changes. Because the factors that control the water vapor amount also control the isotopic fractionation of the air parcel, an accurate measurement of these is of great help to study humidity processes. The measurements from various instruments (cavity ring down spectrometers, ground-based FTIR, atmospheric sounders) have demonstrated this and have been used to examine for instance: air mass mixing (Noone et al., 2011), transport processes (Strong et al., 2007), evaporation of hydro-meteors (Worden et al., 2007), cloud processes (Lee et al., 2011) and intra-seasonal climate variability in the tropics (Kurita et al., 2011; Berkelhammer et al., 2012). The isotopic concentration is commonly expressed as δ values which define the relative deviation with respect to a standard. For example, the concentration in HDO with respect to H_2O

ACPD
12, 13053–13087, 2012

is expressed as:

$$\delta D = 1000 \left(\frac{\frac{HDO}{H_2O}}{VSMOW} - 1 \right), \quad (1)$$

where VSMOW (Vienna Standard Mean Ocean Water) is the reference standard for water isotope ratios (Craig, 1961).

Today, several space-borne instruments measure isotopic ratios with complementary advantages compared to local measurements to capture isotopic variations. The Tropospheric Emission Spectrometer (TES) and the SCanning Imaging Absorption spectroMeter for Atmospheric CartograpHY (SCIAMACHY) instruments have been the first to provide global distributions of δD representative, of the mid-troposphere (Worden et al., 2006, 2007) and the boundary layer (Frankenberg et al., 2009), respectively. Since then, their data have been used extensively. In particular, the inter comparisons of observations with isotopologues-enabled atmospheric general circulation models have demonstrated the added value of such measurements to identify biases in the modeling of the isotopic fractionation and thus to better characterize hydrological processes (Risi et al., 2010a, 2012a,b; Yoshimura et al., 2011).

Two other remote sensing instruments are able to measure the isotopic composition in the troposphere: the Infrared Atmospheric Sounding Interferometer on board MetOp (Clerbaux et al., 2009) and the Thermal And Near infrared Sensor for carbon Observation (TANSO) on board GOSAT (C. Frankenberg, personal communication, 2012). IASI is especially attractive for this purpose, considering its unprecedented spatial coverage and temporal sampling (see below), and the long-term character of the mission with 15 yr of planned continuous data. A first sensitivity study of IASI spectra for measuring δD has been carried out by Herbin et al. (2009). More recently, a comparison between IASI and ground based FTIR measurements has been achieved (Schneider and Hase, 2011).

This paper focuses on the retrieval of δD from IASI spectral radiances. We use a radiative transfer model that is similar to the one used in the Herbin et al. (2009) study.

ACPD
12, 13053–13087, 2012

Their retrieval was based on a simultaneous but independent retrieval of $H_2^{16}O$ and HDO. Here we constrain the retrieval with a full covariance matrix which takes into account the correlations between $H_2^{16}O$ and HDO. This new retrieval methodology is described in Sect. 3. In that section we also extensively characterize the retrievals, in terms of vertical sensitivity and errors. Prior, in Sect. 2, we briefly recall some of the main IASI characteristics. In Sect. 4 we describe the first retrieval results, focusing on the ability of IASI to capture the δD seasonal cycle but also rapid temporal variations at two sites (Izaña 28°18′ N 16°29′ W, and Darwin 12°27′ S 130°50′ E), as well as latitudinal variations on the globe. The retrievals are evaluated by comparing the retrieved values to those modeled by the LMDz-iso General Circulation Model (GCM) (Risi et al., 2010b).

2 IASI observations

IASI is a Fourier transform spectrometer on-board the METOP series of European meteorological polar-orbit satellites. The first model, designed to provide 5 yr of global-scale observations was launched in October 2006. A second and a third instrument will be launched in 2012 and 2016, respectively. IASI measures a large part of the thermal infrared region (645–2760 cm^{-1}) continuously at a medium spectral resolution (0.5 cm^{-1} apodized). It has a low noise of 0.1–0.2 K for a reference blackbody at 280 K, with the lower noise values in the useful range for δD retrievals (Hilton et al., 2012). Primarily designed for operational meteorological soundings with a high level of accuracy, the instrument achieves a global coverage twice a day (orbits crossing the equator at 9.30 and 21.30 local time) with a relatively small pixel size on the ground of 12 km at nadir (diameter of a circular pixel), larger at of nadir viewing angles. With these characteristics IASI makes about 1.3 million measurements per day. Coping with this volume of data is very challenging and requires important computing resources coupled with a fast radiative transfer model (e.g., Hurtmans et al., 2012). In this study we primarily

ACPD
12, 13053–13087, 2012

aim at characterizing the new δD retrievals and therefore we have analyzed observations over selected regions.

The main isotopologues of water ($H_2^{16}O$, $H_2^{18}O$ and HDO) present many spectral lines in the thermal infrared region (Rothman et al., 2003; Toth, 1999). Spectral signatures of these species are well detected by IASI (Herbin et al., 2009) despite the instrument's medium spectral resolution. $\delta^{18}O$ retrievals remain very challenging as its small variations in the atmosphere require high accuracy. δD variations are larger by one order of magnitude and are therefore targeted here. Figure 1 shows part of an IASI spectrum with the spectral windows used in the retrieval (orange curve). These have been chosen to avoid major interferences of CH_4 and N_2O in this range.

3 Retrieval methodology

To retrieve δD from IASI spectral radiances we used the optimal estimation method mainly following the approach proposed by Worden et al. (2006); Schneider et al. (2006). It involves retrieving HDO and H_2O with an a priori covariance matrix which represents the variability of the two species but which also contains information on the correlations between them. The retrieval performed on a log scale allows to better constrain the solution and to minimize the error on the δD profile (Worden et al., 2006; Schneider et al., 2006; Schneider and Hase, 2011). The line-by-line-radiative transfer model software Atmosphit developed at Université Libre de Bruxelles and used in our first attempt to retrieve δD from IASI (Herbin et al., 2009) has been adapted to allow this constrained approach.

While the constrained retrieval approach has been successfully applied on TES measurements (Worden et al., 2006, 2007), ground based measurements (Schneider et al., 2010a, 2006) and a limited number of IASI measurements (Schneider and Hase, 2011), it is anticipated that the retrieval will greatly depend on the choice of retrieval parameters, and in particular on the choice of a priori information. For

ACPD
12, 13053–13087, 2012

instance, Worden et al. (2012) show an improvement in the sensitivity of TES to δD after a change of the retrieval parameters.

3.1 General description

An atmospheric state vector can be related analytically to a corresponding measurement vector which is determined by the physics of the measurement. This relationship can be written as

$$\boldsymbol{y} = \mathbf{F}(\boldsymbol{x}, \boldsymbol{b}) + \boldsymbol{\epsilon}, \tag{2}$$

where $\boldsymbol{y}$ is the measurement vector (in our case, the IASI radiances), $\boldsymbol{\epsilon}$ the instrumental noise, $\boldsymbol{x}$ the state vector which contains the parameters to be retrieved, and $\boldsymbol{b}$ the one that contains all other model parameters impacting the measurement (for instance, interfering species, pressure and temperature profiles). $\mathbf{F}$ is the forward function.

In the case of a linear problem, the maximum a posteriori solution is given by Rodgers (2000) as

$$\hat{\boldsymbol{x}} = \boldsymbol{x}_\mathrm{a} + (\mathbf{K}^T \mathbf{S}_\epsilon^{-1} \mathbf{K} + \mathbf{S}_\mathrm{a}^{-1})^{-1} \mathbf{K}^T \mathbf{S}_\epsilon^{-1} (\boldsymbol{y} - \mathbf{K}\boldsymbol{x}_\mathrm{a}), \tag{3}$$

where $\boldsymbol{x}_\mathrm{a}$ is the a priori state vector, $\mathbf{K}$ is the Jacobian containing the partial derivative of the forward model elements with respect to the state vector element

$$\mathbf{K}_{ij} = \frac{\partial \mathbf{F}_i(x)}{\partial x_j}. \tag{4}$$

$\mathbf{S}_\epsilon$ is the measurement error covariance, and $\mathbf{S}_\mathrm{a}$ is the a priori covariance matrix. The retrieved state is therefore a combination of the measurement and the a priori state inversely weighted by their respective covariance matrices.

Retrieving atmospheric quantities from space measurements is often a non-linear problem which requires numerical method to solve. For a moderately non-linear problem, which is the case here, the best estimate of the state vector can be found by

ACPD
12, 13053–13087, 2012

iteration of

$$\boldsymbol{x}_{i+1} = \boldsymbol{x}_i + (\mathbf{S}_a^{-1} + \mathbf{K}_i^T \mathbf{S}_\epsilon^{-1} \mathbf{K}_i)^{-1} \mathbf{K}_i^T \mathbf{S}_\epsilon^{-1} [\boldsymbol{y} - \mathbf{F}(\boldsymbol{x}_i) + \mathbf{K}_i(\boldsymbol{x}_i - \boldsymbol{x}_a)]. \quad (5)$$

3.2 Retrieval parameters

We retrieve profiles of HDO and $H_2^{16}O$ in ten discretized layers of 1 km thickness. Higher altitudes are not included because in the spectral range used (from 1193 to 1223 cm^{-1} and from 1251 to 1253 cm^{-1}), variations of the state vector at those altitudes do not significantly affect the measurement. This also allows for a faster retrieval. Methane (retrieved as a column) as well as surface temperature are also part of the state vector. The temperature profiles used are the ones retrieved by the Eumetsat Level 2 processor (Schlüssel et al., 2005), estimated with an error of 0.6 to 1.5 K (Pougatchev et al., 2009). Spectrally resolved emissivity values (on IASI sampling) are explicitly considered above land surfaces, using the monthly climatology of Zhou et al. (2011). Only spectra not contaminated by clouds have been considered in this study.

3.3 The a priori information

To retrieve the state vector $\boldsymbol{x}$ from Eq. (2) is in general an ill-posed problem and to obtain a physical meaningful solution we need to constrain the retrieval with a prior information. In the optimal estimation framework, the a priori information is a measure of the knowledge of the state vector prior to the measurement. The usual approach is to assume a Gaussian distribution of the state vector, which can then be characterized by a mean and covariance matrix. The covariance matrix describes to which extent parameters co-vary, for an ensemble of n vectors $\{y_i\}$. It is given by:

$$\mathbf{S}_{i,j} = \sum_{i,j} \{(y_i - \overline{y})(y_j - \overline{y})\}/n^2. \quad (6)$$

Its diagonal elements are the variances of the individual parameters.

ACPD
12, 13053–13087, 2012

Here, our state vector contains H_2O and HDO profiles. Within one profile, different altitude levels are correlated. However, there are also strong correlations between H_2O and HDO. These correlations can be captured in a total covariance matrix $\mathbf{S}_a$, which can naturally be grouped into four sub blocks as

$$\mathbf{S}_a = \begin{pmatrix} \left(\mathbf{S}_{H_2O}\right)_1 & \left(\mathbf{S}_{(H_2O,HDO)}\right)_3 \\ \left(\mathbf{S}_{(HDO,H_2O)}\right)_4 & \left(\mathbf{S}_{HDO}\right)_2 \end{pmatrix}, \quad (7)$$

where the two block $\mathbf{S}_{H_2O}$ and $\mathbf{S}_{HDO}$ are the covariance matrices of the H_2O and HDO, respectively. The matrices $\mathbf{S}_{(H_2O,HDO)} = \mathbf{S}^T_{(HDO,H_2O)}$ contain the correlations between H_2O and HDO.

The choice of the a priori information is critical in the regularization of an ill-posed problem (Rodgers, 2000). The best way to get adequate prior information is to derive the mean and covariance from independent measurements data at high spatial resolution. Only few measurements of δD vertical profiles are available (Ehhalt, 1974; Strong et al., 2007), as are surface measurements (Galewsky et al., 2007; Johnson et al., 2011; Galewsky et al., 2011). There are however not representative for our purpose, which is to retrieve δD profiles over extended areas, covering polar to tropical latitudes. Therefore, to construct a prior probability density function (pdf) we used outputs from the isotopologues-enabled general circulation model LMDz (Risi et al., 2010b) which has demonstrated its capabilities to reasonably well capture water vapor and isotopic distributions at seasonal and intra-seasonal time scales (Risi et al., 2010a, 2012b). These simulations were nudged by ECMWF reanalyzes winds to simulate a day-to-day variability of weather regimes consistent with observations. Mean and covariances of HDO and H_2O profiles as well as covariances between HDO and H_2O were derived from global simulations over a whole year.

We found that the covariance matrix constructed in this way constrained the retrieval too much. This was evident by looking at the retrieval residuals $\boldsymbol{y} - F(\boldsymbol{x}, \boldsymbol{b})$, which were found to be much larger than the instrumental noise. By overly constraining the

ACPD
12, 13053–13087, 2012

retrieval, the retrieval remains too close to the a priori, and not all available information is extracted from the spectrum. To relax the covariance matrices we slightly lowered the correlation between HDO and H_2O. A simple multiplicative factor of 0.9 was applied to all elements of sub-blocks 3 and 4 in the $\mathbf{S}_a$ matrix given by Eq. (7). Figure 2 shows the full a priori covariance matrix obtained (expressed in percent), the corresponding correlation matrix is also shown. The different sub-blocks correspond to Eq. (7). From the covariance matrix one can see (diagonal elements of the first sub-block) that the variability for H_2O varies from 60 % in the first 2 km to 260 % at 7.5 km. The variability for HDO (diagonal of sub-block 3) is quite similar. The construction of the covariance matrix from global data is responsible for this large variability. The correlation matrix exhibits a strong inter levels correlation for each species (sub-blocks 1 and 3).

3.4 Sensitivity diagnostic and error estimation

3.4.1 Sensitivity of the measurement

The Jacobians, which are the derivatives of the measurement vector with respect to the state vector elements (Eq. 4) describe the sensitivity of the measurement to changes of the state vector. In Fig. 3, the Jacobians of HDO and $H_2^{16}O$ are shown in function of altitude in the spectral window used for the retrieval. The altitudes of maximum sensitivities (most negative derivatives corresponding to the largest derivatives) are different for each isotopologue: for HDO maximum sensitivity is achieved between 2 and 6 km, while for $H_2^{16}O$ it is at higher altitudes, between 4 and 7 km, due to saturation at lower altitude at the $H_2^{16}O$ line centers. For $H_2^{16}O$, sensitivity below 4 km remains important but is typically acquired in the selected spectral range in the line wings or between the lines, where continuum absorption dominates.

ACPD
12, 13053–13087, 2012

3.4.2 Sensitivity of the retrieval

The averaging kernel matrix is composed of elements which are the derivatives of the estimated state $\hat{\boldsymbol{x}}$ with respect to the state vector $\boldsymbol{x}$:

$$\mathbf{A} = \frac{\partial \hat{\boldsymbol{x}}}{\partial \boldsymbol{x}}. \quad (8)$$

Averaging kernels are commonly used to evaluate the sensitivity of a retrieval. The matrix can be calculated for total retrieved states vectors (H_2O,HDO) but is not well defined for the calculated δD ratio as a variation of δD cannot uniquely be translated in variations of HDO and H_2O together. Worden et al. (2006) have developed an approach to evaluate the sensitivity of their retrieval to HDO/H_2O. This approach allows for computing the smoothing error covariance matrix for HDO/H_2O ratios from the averaging kernels elements of HDO, H_2O, as well as the cross terms element of the averaging kernels matrix. The covariance of the smoothing error in its general form (for the complete equations used in the calculation of the smoothing error of HDO/H_2O retrieval, see Worden et al., 2006, Sect. 3.2) is expressed as

$$\mathbf{S}_m = (\mathbf{A} - \mathbf{I}_n)\mathbf{S}_e(\mathbf{A} - \mathbf{I}_n)^T, \quad (9)$$

with $\mathbf{S}_e$ the covariance matrix of a real ensemble of states generally approximated by the a priori covariance matrix $\mathbf{S}_a$. Equation (9) explicitly includes a vertical sensitivity through the $\mathbf{A}$ matrix, and it is obvious that the smoothing error decreases when averaging kernels are close to one and/or if the variability in $\mathbf{S}_a$ is small. We therefore use the ratio of the diagonal elements of the smoothing error (adapted for the joint retrieval) to the diagonal elements of the a priori covariance to identify the altitude at which the retrieval is most sensitive. The results are shown in Fig. 4, they correspond to a mean error profile calculated from all error profiles across a latitudinal band. They reveal a very strong reduction in the uncertainty after the retrieval, over the entire altitude range, but especially between 4 and 6 km.

ACPD
12, 13053–13087, 2012

3.4.3 Error estimation from forward simulations

The error of a retrieval can be separated into 3 principal components: (1) the smoothing error, (2) the error due to uncertainties in model parameters, and (3) the error due to the measurement noise. Following this, there are two ways to conduct an error analysis, depending whether one considers the retrieval as an estimate of the true state with an error contribution due to smoothing, or as an estimate of the true state smoothed by the averaging kernels (Rodgers, 2000). The first method requires the knowledge of a real ensemble of states in order to compute the smoothing error. Real ensemble of states are rarely available. In our case it is approximated by the a priori covariance matrix, which is characterized by a large variability, and would lead to largely overestimating the smoothing error (see Eq. 9). Here, we therefore rather estimate errors (2) and (3). To do so, we perform retrievals on a set of simulated IASI spectra (with instrumental noise), representative of different atmospheric conditions. More precisely, 800 spectra have been simulated with temperature and humidity (H_2O and HDO) profiles ranging from standard Arctic profile to tropical standard atmospheres. These various profiles have been extracted from LMDz-iso simulations. We then compared the retrieved profiles with the real ones, smoothed with the averaging kernels to remove the contribution of the smoothing error. The smoothed profiles of water mixing ratios ($\boldsymbol{q}_{\mathrm{mAK}}$) are obtained as

$$\log(\boldsymbol{q}_{\mathrm{mAK}}) = \mathbf{A}_{\mathrm{hh}} \cdot \log(\boldsymbol{q}_{\mathrm{m}}) + (\mathbf{I}_{\mathrm{n}} - \mathbf{A}_{\mathrm{hh}}) \cdot \log(\boldsymbol{q}_{\mathrm{p}}), \quad (10)$$

where $\boldsymbol{q}$ is the vector of water mixing ratios, for the real (subscript m) or the a priori profiles (subscript p). $\mathbf{A}_{\mathrm{hh}}$ are the averaging kernels of H_2O. For δD, the smoothing also requires involving the cross terms elements of the averaging kernels matrix. Following Risi et al. (2012b) the real ratio $\boldsymbol{R} = \mathrm{HDO}/\boldsymbol{q}$ as seen with the sensitivity of our retrieval

ACPD
12, 13053–13087, 2012

is

$$\log(\boldsymbol{R}_{\mathrm{mAK}}) = \log(\boldsymbol{R}_{\mathrm{p}}) + \left[(\mathbf{A}_{\mathrm{dd}} - \mathbf{A}_{\mathrm{hd}}) \cdot (\log(\mathrm{HDO}_{\mathrm{m}}) - \log(\mathrm{HDO}_{\mathrm{p}})) - (\mathbf{A}_{\mathrm{hh}} - \mathbf{A}_{\mathrm{dh}}) \cdot (\log(\boldsymbol{q}_{\mathrm{m}}) - \log(\boldsymbol{q}_{\mathrm{p}}))\right]. \quad (11)$$

An extensive study of the different error sources on δD retrievals from IASI (Schneider and Hase, 2011) shows that the two largest contributions to the total error are due to the measurement noise and to the uncertainty on temperature profile, while other sources of error (spectroscopy, interfering species, surface temperature and emissivity) contribute to less than 4 ‰ to the total error. For our error estimation the two major contributions are evaluated. First, we performed retrievals on simulated spectra with identical temperature profiles in the simulation and in the retrieval. Doing so, there is no uncertainty in the temperature profile and the errors between retrieved profiles and original ones are only due to the measurement noise. Then, to evaluate the error due to the uncertainties in the temperature profile, we performed the retrievals on simulated spectra with altered temperature profiles. We considered an uncertainty on the temperature of 1.5 K from 0 to 2 km and 0.6 K for the rest of the atmosphere, based on first validation results of the EUMETSAT L2 temperature profiles (Pougatchev et al., 2009). Differences between original and retrieved profiles give the error due to measurement noise and uncertainties in the temperature profiles, which can then be isolated. Figure 5 shows the total error profile expressed as the standard deviations of the difference between original and retrieved profiles and its two main contributions. It shows that the total error is always below 50 ‰ in the altitude range 1–7 km, decreasing to below 40 ‰ between 2 and 5 km. The measurement noise is strongly dominating the error budget throughout the troposphere but especially above 1 km.

To determine the altitude range where our retrieval is the most sensitive, we mainly consider Fig. 4 which indicates a maximum of reduction in error between 3 and 6 km. This range also corresponds to the best compromise in the overlapping of H_2O and H_2O maximum measurement sensitivities (see Fig. 3). However this is not in agreement

ACPD
12, 13053–13087, 2012

with our theoretical error estimation which indicates a minimization of error between 1 and 5 km. This can be explained by the influence of the a priori covariance matrix which is more stringent in the lower atmosphere. This becomes clear when looking at the correlation between retrieved profiles and the original input profiles, which shows a maximum correlation again between 3 and 6 km.

4 Spatio-temporal variability of δD retrievals

To evaluate the performance of our retrievals on real spectra, we present in this section retrievals at two sites characterized by very different hydrological regimes; namely a subsidence site (Izaña) and a convective site (Darwin) for the full year 2010. In addition we provide δD variations along a latitudinal gradient from −60° to 60°.

The evaluation is carried out by comparing the retrieved δD values, and their time and spatial variations with the LMDz HDO and H_2O outputs, smoothed by the averaging kernels of the retrieval (Eqs. 10 and 11). Note that due to the model grid size, the averaging kernels used here correspond to the daily mean averaging kernels of the retrievals contained in the LMDz grid box (grid size of 2.5° of latitude and 3.75° of longitude). We have verified that the daily variability and the difference between land and sea averaging kernels are small enough to not affect the smoothing between 3 and 6 km.

To evaluate the pattern correspondences between observations and model we first report in Table 1 some statistical diagnostics (Taylor, 2001) for the three studied cases. In the table, we report the correlation coefficient (r), the standard deviations of the LMDz-iso and IASI datasets (σ_{LMDz} and σ_{IASI}), the ratio of their standard deviations ($R_\sigma = \sigma_{\mathrm{LMDz}}/\sigma_{\mathrm{IASI}}$), the overall bias ($E$), and N, the number of observations. These statistics are used to support the discussion in the next two subsections.

ACPD
12, 13053–13087, 2012

4.1 Annual and day-to-day variability at Izaña and Darwin

The principal advantage of IASI over other satellite sounders measuring δD is its spatial and temporal coverage. Indeed IASI provides global coverage twice a day, which allows studying day to day variability of isotopic distributions. This is not possible with TES and SCIAMACHY instruments as they need several days to achieve global coverage.

Retrieved δD and H_2O time-series for the Darwin and Izaña sites are shown respectively in Figs. 6 and 7 together with LMDz-iso simulations (blue crosses). The studied zones extend from 128° E to 133° E, 14° S to 10° S for Darwin, and from 18.5° W to 14.5° W, 26° N to 30° N for Izaña. Plotted values are integrated δD values for the 3–6 km layer. Daily-averaged retrieved values (full red circles) have been spatially averaged over the model grid box. A 30 days smoothing filter applied on modeled (thick blue line) and observed (thick red line) values is also plotted to highlight the underlying seasonal pattern. We discuss hereafter, the seasonal variations and then the short term variations, which strongly overlap the seasonal cycle.

4.1.1 Seasonal variability

Darwin is a tropical site with two distinct seasons: a dry season, from May to October (Austral winter), and a wet season from November to April (Austral summer) characterized by cloudy and rainy conditions caused by large scale convective processes. Figure 6, which gives the 2010 time series of δD, shows a well-marked seasonal cycle (80 ‰ amplitude) with lower retrieved δD values in winter (a minimum of −200 ‰ in June) and with high values in summer (maximum of −120 ‰ in February). This is in excellent agreement with LMDz-iso, which shows a ±95 ‰ amplitude with similar maximum in February (−130 ‰) and a minimum in June (−225 ‰). The comparison with LMDz is particularly remarkable when considering the very strong similarity in the timing and relative variations for both H_2O and δD. At Darwin, the isotopic composition is mainly sensitive to two overlapping effects: (1) a seasonality effect with low δD values in austral winter when subsidence is important, in that case H_2O and δD will

ACPD
12, 13053–13087, 2012

be correlated and (2) an effect due to the convection that contributes to deplete the air mass in HDO in that case, δD and H_2O trends will be anti-correlated. This second effect is clearly visible on the Darwin time series in January-mid February where H_2O reaches a maximum while δD reaches a minimum.

Izaña, located in the northern Atlantic Ocean at subtropical latitudes, is characteristic of a subsidence zone with a very dry climate. The time series for Izaña is shown in Fig. 7. A seasonal cycle is clearly identifiable with low δD values in winter (min values of −250 ‰), and high values in summer (max values of −150 ‰). The general agreement between IASI and LMDz is good, but contrary to what we observed at Darwin, there are some noticeable differences in the seasonal and intra-seasonal variations. In particular, the seasonality (difference between summer months and winter months) retrieved with IASI is larger than LMDz: in winter LMDz simulates higher δD values than IASI and in summer model simulations are lower. In annual mean this translates into a −15 ‰ bias of IASI compared to the model. While these differences in δD could be due in part to the retrievals, we believe that they essentially come from the model, which has been shown before to underestimate the δD seasonality in the subtropics (Risi et al., 2012b). Note that the differences do not apply to H_2O (bottom panel of Fig. 7) for which observations and simulations are in very good agreement during the winter months, but where IASI retrievals are systematically higher than the model from May to the end of September. In June, the strong increase of δD, followed by the increase of water amount probably indicates that subsidence has decreased.

4.1.2 Short term variability

Figures 6 and 7 reveal strong day-to-day-variations within the broader seasonal cycle at the two locations. For instance, in a few days δD can vary by 100 ‰ (e.g. at Darwin in June or Izaña in October), which is similar to the amplitude of the seasonal cycle. A remarkable result of this preliminary comparison comes from the general excellent agreement between IASI and model δD values on a daily basis. At Darwin the differences between LMDz-iso and IASI (middle panel of Fig. 6) are below 50 ‰ (91 % of

ACPD
12, 13053–13087, 2012

the points) and below 25 ‰ (64 % of the points). We note however a tendency of IASI to have larger variability (for example in April–May), as further discussed below. The bias of annual mean is below 2 ‰.

At Izaña, the differences are larger and vary seasonally, which is due to the seasonal bias already highlighted in Sect. 4.1.1. However, we see that LMDz-iso and IASI tend to agree better in the magnitude of the variability at Izaña (ratio of standard deviation of 1, see Table 1) than at Darwin, where the variability in the retrieved value (33.5 ‰) is higher by 3.5 ‰ than that from the model (30 ‰). This is also seen from Fig. 8, where retrieved δD (daily averaged value in the grid box) are plotted versus model δD values. This figure also allows for a visualization of the correlation pattern between the two different data sets. At Izaña, we find a correlation coefficient of 0.5 (see also Table 1), when taking all observations into account. If we only consider the IASI measurements for which the daily variability in the grid box is below 35 ‰, the correlation coefficient increases to 0.64 with a slope still close to 1. At Darwin this effect is not observed, the slope of 1.22 indicates a larger amplitude of the variations of IASI as compared to the model (similar indication than variances ratio). The correlation coefficient is also relatively significant (0.55) here (Fig. 8 and Table 1).

Note that Yoshimura et al. (2011), have presented a similar comparison between TES retrievals and the IsoGCM model. Contrary to what we find here, they suggest that TES observations underestimate the magnitude of the short term variability. We believe that the better agreement found with IASI compared to model data could be due to the specific a priori constraint applied, which could be less stringent that the one used for TES retrievals.

4.2 Spatial variability along a latitudinal gradient

In addition to the temporal variations, we have examined the ability of IASI to capture the spatial variability of δD by considering a latitudinal band from −60° to 60°. Figure 9 shows the δD and H_2O latitudinal distributions representative of the 3–6 km layer averaged on LMDz-iso grid boxes (from −30° to −25° in longitude above ocean surfaces)

ACPD
12, 13053–13087, 2012

for the first 15 days of January 2010. As expected, the retrieved δD are largest near the equator (mean value of −140 ‰) and decrease polewards to reach a minimum value of −350 ‰ at 56° S (gradient of −210 ‰). Local maxima are observed in the subtropics for both H_2O and δD distributions but with a significant phase shift; with δD maxima being localized at higher latitudes than H_2O. This is explained by the fact that at high and mid latitudes, isotopic composition follows a Rayleigh type distillation while at subtropical latitudes, the isotopic composition is sensitive to mixing processes, which will lead to an enrichment of the air parcel for a same water amount (Galewsky and Hurley, 2010). In the tropics the convection contributes to deplete the air masses in the heavier isotopologues. These processes are responsible for the smoother behavior of δD compared to H_2O.

The retrieved values are in very good agreements with model values for water vapour (correlation coefficient of 0.90, ratio of standard deviations of 1.05 and a moist bias of 0.32 g kg^{-1}). The observed variations are in phase with the simulated ones. The only noticeable differences are the lower water concentration simulated by LMDz at the equator and the higher concentration simulated in the southern subtropics.

The comparison of the δD gradients is also very good when looked at globally, with a correlation coefficient of 0.83. However, large differences occur in the magnitude of the variations (ratio of standard deviations of 1.38, LMDz standard deviation (74.02 ‰) being significant larger than IASI one (53.46 ‰)). The timing of the variations is also quite good. The major differences occur in subtropical regions where LMDz systematically simulates higher δD values than IASI and where correspondence between the LMDz and IASI timing is not observed. Noticeable differences also appear between 45° and 60° where LMDz values are much lower than retrieved ones, difference reaches 100 ‰ around 54°. Added to the underestimation of the seasonality at subtropical latitudes, Risi et al. (2012b) have identified the underestimation of the latitudinal gradient (zonal annual mean) and in particular a pronounced high bias in δD at subtropical latitudes as robust features of the model. While we don't observe the underestimation of latitudinal gradient by LMDz our comparison tends to confirm a misrepresentation

ACPD
12, 13053–13087, 2012

of the processes affecting δD in the subtropics. A detailed study of the IASI to model differences is beyond the scope of the present paper and will be the subject of forthcoming analyses.

5 Conclusions

We have described a new joint retrieval methodology for H_2O and HDO from IASI radiances spectra. Based on optimal estimation, the method is different from our previous work in that it constrains the retrievals by explicitly introducing the correlations in the concentrations of the two species inside the a priori covariance matrix $\mathbf{S}_a$. It was built from a global set of daily vertical profiles from the LMDz-iso GCM representative of the whole year, and therefore shows large variability around the a priori, which are the average profiles of H_2O and HDO. The $\mathbf{S}_a$ matrix was slightly modified to decrease the model correlations between the two species. The spectral range for the retrievals was set to 1193 to 1253 cm^{-1} with a gap between 1223 and 1251 cm^{-1}. With these settings, we show that IASI provides maximum sensitivity simultaneously to HDO and H_2O in the free troposphere with error on the retrieved δD vertical profiles lower than 40 ‰ between 2 and 5 km. Considering an individual retrieval, the error on δD in the 3–6 km layer is 38 ‰ and was shown to be dominated by the measurement noise.

The seasonal variability of the IASI retrieved δD was examined at two locations for the year 2010, and compared to that of the LMDz-iso model. We found a general excellent agreement in the magnitude of the seasonal pattern in comparison with the model, although differences exist depending on the location. While at Izaña a clear seasonal bias has been identified (overall bias of 15 ‰), the bias at Darwin is insignificant (< 2 ‰). Beyond the seasonal cycle, we have demonstrated the good performance of IASI to capture short-term variations of δD (e.g. day-to-day variations) despite significant differences in the amplitude of variations estimated from the model and the retrieved one at Darwin. It is worthwhile mentioning that IASI is currently the only satellite sounder which allows monitoring δD on a daily basis. Finally, we have investigated

ACPD
12, 13053–13087, 2012

the performance of the retrievals by analyzing the δD results for a 5° wide longitude band from −60° S to 60° N for the first 15 days of January. We show that the retrieved values are in very good agreement with the model but while the overall agreement is remarkable (correlation coefficient of 0.83), noticeable differences occur. These are a significant deviation between LMDz and IASI at subtropical latitudes and the lower δD values simulated beyond the 45° latitudes. While differences highlighted in this study could be due to retrieval issues, they confirm previously documented shortcomings of the model.

More generally, the very good performance of the new retrieval method highlights further the exceptional potential of IASI to contribute to the understanding of hydrological processes.

Acknowledgements. IASI has been developed and built under the responsibility of the Centre National d'Etudes Spatiales (CNES, France). It is flown onboard the MetOp satellites as part of the EUMETSAT Polar System. The IASI L1 data are received through the EUMETCast near real time data distribution service. The research in Belgium was funded by the "Communauté Française de Belgique – Actions de Recherche Concertées", the Fonds National de la Recherche Scientifique (FRS-FNRS F.4511.08), the Belgian Science Policy Office and the European Space Agency (ESA-Prodex C90-327). L. Clarisse and P.-F. Coheur are respectively Postdoctoral Researcher (Chargé de Recherches) and Research Associate (Chercheur Qualifié) with F.R.S.-FNRS. C. Clerbaux is grateful to CNES for scientific collaboration and financial support.

References

Berkelhammer, M., Risi, C., Kurita, N., and Noone, D. C.: The moisture source sequence for the Madden-Julian Oscillation as derived from satellite retrievals of HDO and H_2O, J. Geophys. Res., 117, D03106, doi:10.1029/2011JD016803, 2012. 13055

Bony, S., Colman, R., Kattsov, V., Allan, R., Bretherton, C., Dufresne, J., Hall, A., Hallegatte, S., Holland, M., Ingram, V., Randall, D., Soden, B., Tselioudis, G., and Webb, M.: How Well

ACPD

12, 13053–13087, 2012

Do We Understand and Evaluate Climate Change Feedback Processes?, J. Climate, 19, 3445–3482, 2006. 13055

Clerbaux, C., Boynard, A., Clarisse, L., George, M., Hadji-Lazaro, J., Herbin, H., Hurtmans, D., Pommier, M., Razavi, A., Turquety, S., Wespes, C., and Coheur, P.-F.: Monitoring of atmospheric composition using the thermal infrared IASI/MetOp sounder, Atmos. Chem. Phys., 9, 6041–6054, doi:10.5194/acp-9-6041-2009, 2009. 13056

Craig, H.: Isotopic Variations in Meteoric Waters, Science, 133, 1702–1703, doi:10.1126/science.133.3465.1702, 1961. 13056

Ehhalt, D. H.: Vertical profiles of HTO, HDO, and H_2O in the Troposphere, NCAR-TN/STR-100, Natl. Cent. for Atmos. Res., Boulder, Colo., 1974. 13061

Frankenberg, C., Yoshimura, K., Warneke, T., Aben, I., Butz, A., Deutscher, N., Griffith, D., Hase, F., Notholt, J., Schneider, M., Schrijver, H., and Rockmann, T.: Dynamic Processes Governing Lower-Tropospheric HDO/H_2O Ratios as Observed from Space and Ground, Science, 325, 1374–1377, doi:10.1126/science.1173791, 2009. 13056

Frierson, D. M. W.: The Dynamics of Idealized Convection Schemes and Their Effect on the Zonally Averaged Tropical Circulation, J. Atmos. Sci., 64, 1959–1976, doi:10.1175/JAS3935.1, 2007. 13055

Galewsky, J. and Hurley, J. V.: An advection-condensation model for subtropical water vapor isotopic ratios, J. Geophys. Res., 115, D16116, doi:10.1029/2009JD013651, 2010. 13070

Galewsky, J., Strong, M., and Sharp, Z. D.: Measurements of water vapor D/H ratios from Mauna Kea, Hawaii, and implications for subtropical humidity dynamics, Geophys. Res. Lett., 34, L22808, doi:10.1029/2007GL031330, 2007. 13061

Galewsky, J., Rella, C., Sharp, Z., Samuels, K., and Ward, D.: Surface measurements of upper tropospheric water vapor isotopic composition on the Chajnantor Plateau, Chile, Geophys. Res. Lett., 38, L17803, doi:10.1029/2011GL048557, 2011. 13061

Herbin, H., Hurtmans, D., Clerbaux, C., Clarisse, L., and Coheur, P.-F.: $H_2^{16}O$ and HDO measurements with IASI/MetOp, Atmos. Chem. Phys., 9, 9433–9447, doi:10.5194/acp-9-9433-2009, 2009. 13056, 13058

Hilton, F., Armante, R., August, T., Barnet, C., Bouchard, A., Camy-Peyret, C., Capelle, V., Clarisse, L., Clerbaux, C., Coheur, P.-F., Collard, A., Crevoisier, C., Dufour, G., Edwards, D., Faijan, F., Fourrié, N., Gambacorta, A., Goldberg, M., Guidard, V., Hurtmans, D., Illingworth, S., Jacquinet-Husson, N., Kerzenmacher, T., Klaes, D., Lavanant, L., Masiello, G., Matricardi, M., McNally, A., Newman, S., Pavelin, E., Payan, S., Péquignot, E., Peyridieu, S.,

ACPD
12, 13053–13087, 2012

Phulpin, T., Remedios, J., Schlüssel, P., Serio, C., Strow, L., Stubenrauch, C., Taylor, J., Tobin, D., Wolf, W., and Zhou, D.: Hyperspectral Earth Observation from IASI: Five Years of Accomplishments, Bull. Amer. Meteor. Soc., 93, 347–370, doi:10.1175/BAMS-D-11-00027.1, 2012. 13057

Hurtmans, D., Coheur, P.-F., Wespes, C., Clarisse, L., Scharf, O., Clerbaux, C., Hadji-Lazaro, J., George, M., and Turquety, S.: FORLI radiative transfer and retrieval code for IASI, J. Quant. Spectrosc. Rad., 113, 1391–1408, doi:10.1016/j.jqsrt.2012.02.036, 2012. 13057

Johnson, L. R., Sharp, Z. D., Galewsky, J., Strong, M., Van Pelt, A. D., Dong, F., and Noone, D.: Hydrogen isotope correction for laser instrument measurement bias at low water vapor concentration using conventional isotope analyses: application to measurements from Mauna Loa Observatory, Hawaii, Rapid Commun. Mass Sp., 25, 608–616, doi:10.1002/rcm.4894, 2011. 13061

Kang, S. M., Held, I. M., Frierson, D. M. W., and Zhao, M.: The Response of the ITCZ to Extratropical Thermal Forcing: Idealized Slab-Ocean Experiments with a GCM, J. Climate, 21, 3521–3532, doi:10.1175/2007JCLI2146.1, 2008. 13055

Kiehl, J. T. and Trenberth, K. E.: Earth's Annual Global Mean Energy Budget, Bull. Amer. Meteor. Soc., 78, 197–208, doi:10.1175/1520-0477(1997)078<0197:EAGMEB>2.0.CO;2, 1997. 13055

Kurita, N., Noone, D., Risi, C., Schmidt, G. A., Yamada, H., and Yoneyama, K.: Intraseasonal isotopic variation associated with the Madden-Julian Oscillation, J. Geophys. Res., 116, D24101, doi:10.1029/2010JD015209, 2011. 13055

Lee, J., Worden, J., Noone, D., Bowman, K., Eldering, A., LeGrande, A., Li, J.-L. F., Schmidt, G., and Sodemann, H.: Relating tropical ocean clouds to moist processes using water vapor isotope measurements, Atmos. Chem. Phys., 11, 741–752, doi:10.5194/acp-11-741-2011, 2011. 13055

Noone, D., Galewsky, J., Sharp, Z. D., Worden, J., Barnes, J., Baer, D., Bailey, A., Brown, D. P., Christensen, L., Crosson, E., Dong, F., Hurley, J. V., Johnson, L. R., Strong, M., Toohey, D., Van Pelt, A., and Wright, J. S.: Properties of air mass mixing and humidity in the subtropics from measurements of the D/H isotope ratio of water vapor at the Mauna Loa Observatory, J. Geophys. Res., 116, D22113, doi:10.1029/2011JD015773, 2011. 13055

Pougatchev, N., August, T., Calbet, X., Hultberg, T., Oduleye, O., Schlüssel, P., Stiller, B., Germain, K. St., and Bingham, G.: IASI temperature and water vapor retrievals – error

ACPD
12, 13053–13087, 2012

assessment and validation, Atmos. Chem. Phys., 9, 6453–6458, doi:10.5194/acp-9-6453-2009, 2009. 13060, 13065

Randall, D. A., Harshvardhan, Dazlich, D. A., and Corsetti, T. G.: Interactions among Radiation, Convection, and Large-Scale Dynamics in a General Circulation Model, J. Atmos. Sci., 46, 1943–1970, doi:10.1175/1520-0469(1989)046<1943:IARCAL>2.0.CO;2, 1989. 13055

Risi, C., Bony, S., Vimeux, F., Frankenberg, C., Noone, D., and Worden, J.: Understanding the Sahelian water budget through the isotopic composition of water vapor and precipitation, J. Geophys. Res., 115, D24110, doi:10.1029/2010JD014690, 2010a. 13056, 13061

Risi, C., Bony, S., Vimeux, F., and Jouzel, J.: Water-stable isotopes in the LMDZ4 general circulation model: Model evaluation for present-day and past climates and applications to climatic interpretations of tropical isotopic records, J. Geophys. Res., 115, D12118, doi:10.1029/2009JD013255, 2010b. 13057, 13061

Risi, C., Noone, D., Worden, J., Frankenberg, C., Stiller, G., Kiefer, M., Funke, B., Walker, K., Bernath, P., Schneider, M., Bony, S., Lee, J., Brown, D., and Sturm, C.: Process-evaluation of tropospheric humidity simulated by general circulation models using water vapor isotopic observations: 2. Using isotopic diagnostics to understand the mid and upper tropospheric moist bias in the tropics and subtropics, J. Geophys. Res., 117, D05304, doi:10.1029/2011JD016623, 2012a. 13056

Risi, C., Noone, D., Worden, J., Frankenberg, C., Stiller, G., Kiefer, M., Funke, B., Walker, K., Bernath, P., Schneider, M., Wunch, D., Sherlock, V., Deutscher, N., Griffith, D., Wennberg, P. O., Strong, K., Smale, D., Mahieu, E., Barthlott, S., Hase, F., García, O., Notholt, J., Warneke, T., Toon, G., Sayres, D., Bony, S., Lee, J., Brown, D., Uemura, R., and Sturm, C.: Process-evaluation of tropospheric humidity simulated by general circulation models using water vapor isotopologues: 1. Comparison between models and observations, J. Geophys. Res., 117, D05303, doi:10.1029/2011JD016621, 2012b. 13056, 13061, 13064, 13068, 13070

Rodgers, C. D.: Inverse methods for atmospheric sounding: theory and practise, World Scientific, 2000. 13059, 13061, 13064

Rothman, L. S., Barbe, A., Chris Benner, D., Brown, L. R., Camy-Peyret, C., Carleer, M. R., Chance, K., Clerbaux, C., Dana, V., Devi, V. M., Fayt, A., Flaud, J. M., Gamache, R. R., Goldman, A., Jacquemart, D., Jucks, K. W., Lafferty, W. J., Mandin, J. Y., Massie, S. T., Nemtchinov, V., Newnham, D. A., Perrin, A., Rinsland, C. P., Schroeder, J., Smith, K. M., Smith, M. A. H., Tang, K., Toth, R. A., Vander Auwera, J., Varanasi, P., and Yoshino, K.:

ACPD

12, 13053–13087, 2012

The HITRAN molecular spectroscopic database: edition of 2000 including updates through 2001, J. Quant. Spectrosc. Ra., 82, 5–44, 2003. 13058
Schlüssel, P., Hultberg, T. H., Phillips, P. L., August, T., and Calbet, X.: The operational IASI Level 2 processor, Advances in Space Research, 36, 982–988, 2005. 13060
Schmidt, G. A., Ruedy, R. A., Miller, R. L., and Lacis, A. A.: Attribution of the present-day total greenhouse effect, J. Geophys. Res., 115, D20106, doi:10.1029/2010JD014287, 2010. 13055
Schneider, M. and Hase, F.: Optimal estimation of tropospheric H_2O and δD with IASI/METOP, Atmos. Chem. Phys., 11, 11207–11220, doi:10.5194/acp-11-11207-2011, 2011. 13056, 13058, 13065
Schneider, M., Hase, F., and Blumenstock, T.: Ground-based remote sensing of HDO/H_2O ratio profiles: introduction and validation of an innovative retrieval approach, Atmos. Chem. Phys., 6, 4705–4722, doi:10.5194/acp-6-4705-2006, 2006. 13058
Schneider, M., Yoshimura, K., Hase, F., and Blumenstock, T.: The ground-based FTIR network's potential for investigating the atmospheric water cycle, Atmos. Chem. Phys., 10, 3427–3442, doi:10.5194/acp-10-3427-2010, 2010a. 13058
Schneider, T., O'Gorman, P. A., and Levine, X. J.: Water vapor and the dynamics of climate changes, Rev. Geophys., 48, RG3001, doi:10.1029/2009RG000302, 2010b. 13055
Sherwood, S. C., Roca, R., Weckwerth, T. M., and Andronova, N. G.: Tropospheric water vapor, convection, and climate, Rev. Geophys., 48, RG2001, doi:10.1029/2009RG000301, 2010. 13055
Soden, B. J. and Held, I. M.: An Assessment of Climate Feedbacks in Coupled Ocean Atmosphere Models, J. Climate, 19, 3354–3360, doi:10.1175/JCLI3799.1, 2006. 13055
Strong, M., Sharp, Z. D., and Gutzler, D. S.: Diagnosing moisture transport using D/H ratios of water vapor, Geophys. Res. Lett., 34, L03404, doi:10.1029/2006GL028307, 2007. 13055, 13061
Taylor, K. E.: Summarizing multiple aspects of model performance in a single diagram, J. Geophys. Res., 106, 7183–7192, doi:10.1029/2000JD900719, 2001. 13066
Toth, R. A.: HDO and D_2O low pressure, long path spectra in the 600–3100 cm^{-1} Region: I. HDO line positions and strengths, J. Mol. Spectrosc., 195, 73–97, 1999. 13058
Worden, J., Bowman, K., Noone, D., Beer, R., Clough, S., Eldering, A., Fisher, B., Goldman, A., Gunson, M., Herman, R., Kulawik, S. S., Lampel, M., Luo, M., Osterman, G., Rinsland, C., Rodgers, C., Sander, S., Shephard, M., and Worden, H.: Tropospheric Emission

ACPD
12, 13053–13087, 2012

Spectrometer observations of the tropospheric HDO/H_2O ratio: Estimation approach and characterization, J. Geophys. Res., 111, D16309, doi:10.1029/2005JD006606, 2006. 13056, 13058, 13063

Worden, J., Noone, D., and Bowman, K.: Importance of rain evaporation and continental convection in the tropical water cycle, Nature, 445, 528–532, doi:10.1038/nature05508, 2007. 13055, 13056, 13058

Worden, J., Kulawik, S., Frankenberg, C., Payne, V., Bowman, K., Cady-Peirara, K., Wecht, K., Lee, J.-E., and Noone, D.: Profiles of CH_4, HDO, H_2O, and N_2O with improved lower tropospheric vertical resolution from Aura TES radiances, Atmos. Meas. Tech., 5, 397–411, doi:10.5194/amt-5-397-2012, 2012. 13059

Yoshimura, K., Frankenberg, C., Lee, J., Kanamitsu, M., Worden, J., and Röckmann, T.: Comparison of an isotopic atmospheric general circulation model with new quasi-global satellite measurements of water vapor isotopologues, J. Geophys. Res., 116, D19118, doi:10.1029/2011JD016035, 2011. 13056, 13069

Zhang, R., Kang, S. M., and Held, I. M.: Sensitivity of Climate Change Induced by the Weakening of the Atlantic Meridional Overturning Circulation to Cloud Feedback, J. Climate, 23, 378–389, doi:10.1175/2009JCLI3118.1, 2010. 13055

Zhou, D., Larar, A., Liu, X., Smith, W., Strow, L., Yang, P., Schlüssel, P., and Calbet, X.: Global Land Surface Emissivity Retrieved From Satellite Ultraspectral IR Measurements, IEEE Trans. Geosci. Remote Sens, 49, 1277–1290, doi:10.1109/TGRS.2010.2051036, 2011. 13060

ACPD

12, 13053–13087, 2012

Table 1. Statistics between LMDz-iso simulated and IASI retrieved values for the different datasets presented. r is the correlation coefficient, σ_{LMDz} and σ_{IASI} are the standard deviations of LMDz-iso and IASI respectively, R_σ the ratio of standard deviations with $R_\sigma = \sigma_{\mathrm{LMDz}}/\sigma_{\mathrm{IASI}}$, E is the overall bias ($E = \bar{\mathrm{LMDz}} - \bar{\mathrm{IASI}}$), and N the number of values considered. The standard deviations as the overall bias are expressed in permil and in $\mathrm{g\,kg^{-1}}$ for δD and H_2O, respectively.

		r	σ_{LMDz}	σ_{IASI}	R_σ	E	N
Izaña	δD	0.50	44.57	44.57	1.00	−15.38	324
	H_2O	0.62	0.83	1.00	0.83	0.28	324
Darwin	δD	0.55	29.94	33.47	0.89	−1.92	267
	H_2O	0.69	1.35	1.43	0.94	−0.36	267
Latitudinal Gradient	δD	0.83	74.02	53.46	1.38	−3.41	48
	H_2O	0.90	0.99	0.94	1.05	0.32	48

ACPD
12, 13053–13087, 2012

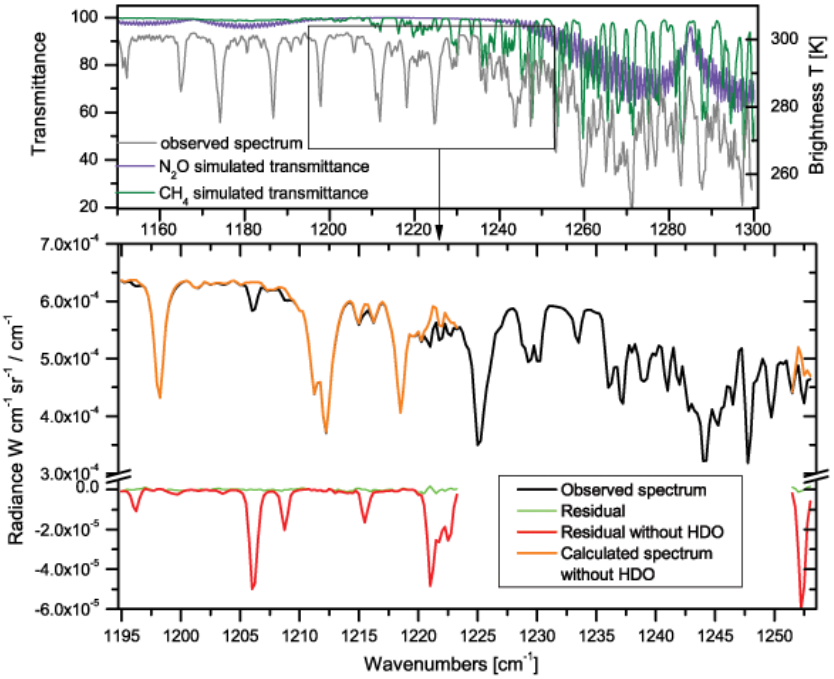

Fig. 1. Spectral window used in the retrieval. Top panel: IASI spectra (black curve) in brigthness temperature with the spectral signature of CH_4 and N_2O. Bottom panel: zoom on the spectral channels used in the retrieval (orange curve) the gap between 1223 and 1251 cm^{-1} avoids major CH_4 and N_2O interferences.

ACPD
12, 13053–13087, 2012

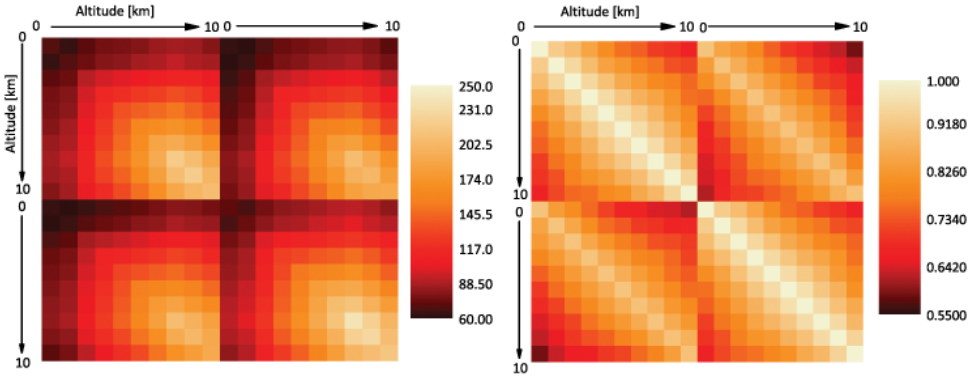

Fig. 2. A priori covariance matrix expressed in percent (left) and the corresponding correlation matrix (right).

ACPD
12, 13053–13087, 2012

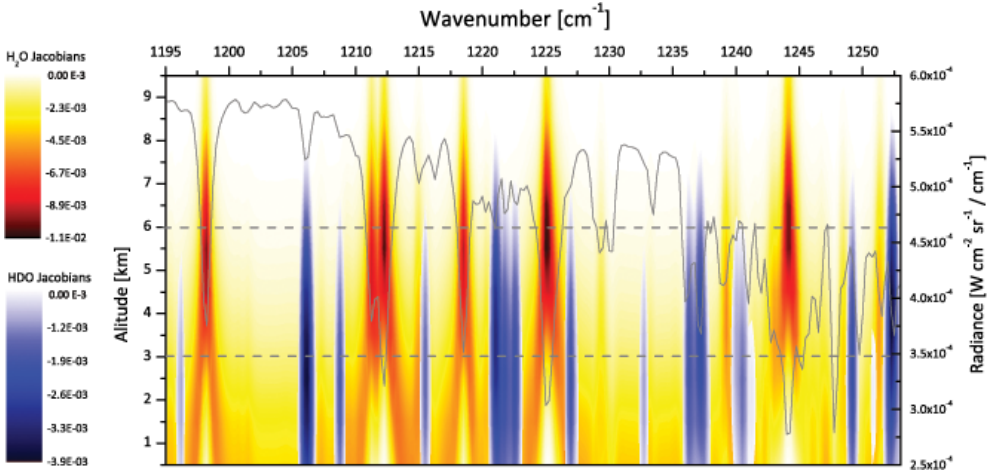

Fig. 3. Jacobians of H_2O (yellow to dark red) and HDO (light blue to dark blue) as function of altitude and wavenumber. The smallest derivatives values indicate the maximum sensitivities. The gray dashed lines indicate the altitude of maximum sensitivity for both.

ACPD
12, 13053–13087, 2012

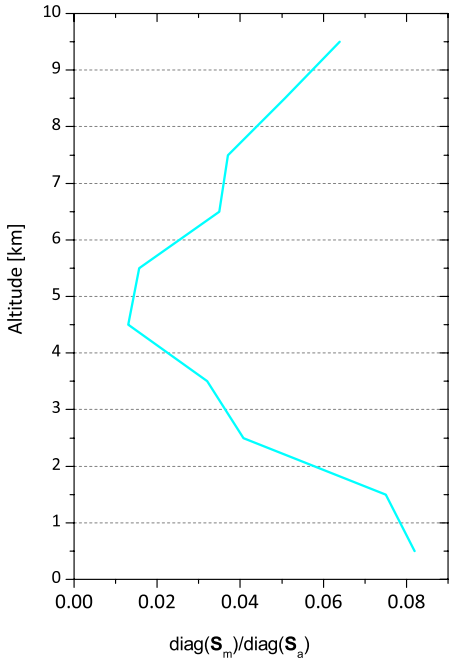

Fig. 4. Ratio of the square root of the diagonal elements of the smoothing error covariance matrix to the square root of the diagonal elements of the a priori covariance matrix.

ACPD
12, 13053–13087, 2012

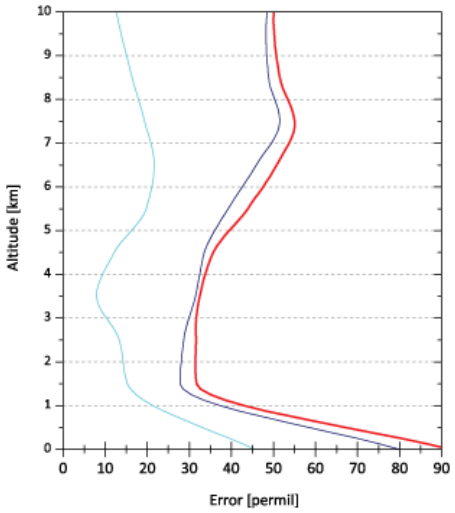

Fig. 5. Total error profile on δD in ‰ (red line) with the contributions due to the measurement noise (blue line) and to the uncertainties in the temperature profile (cyan line).

ACPD
12, 13053–13087, 2012

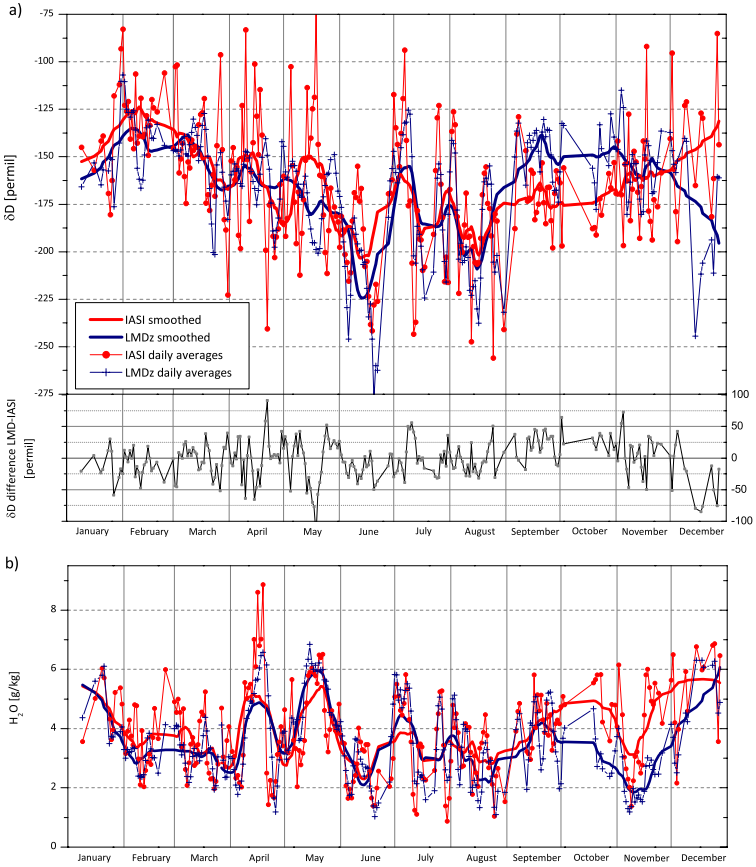

Fig. 6. Time series at the Darwin site for the year 2010 for the 3–6 km layer. **(a)** Top pannel: IASI δD daily averages (red circles and line), are compared to corresponding LMDz-iso simulations (blue crosses and line). A Savitzky-Golay smoothing filter has been applied (thick lines) to highlight seasonal and intra-seasonal pattern. **(b)** Same as **(a)** but for specific humidity in g kg^{-1}.

ACPD
12, 13053–13087, 2012

Mid-tropospheric δD observations from IASI/MetOp

J.-L. Lacour et al.

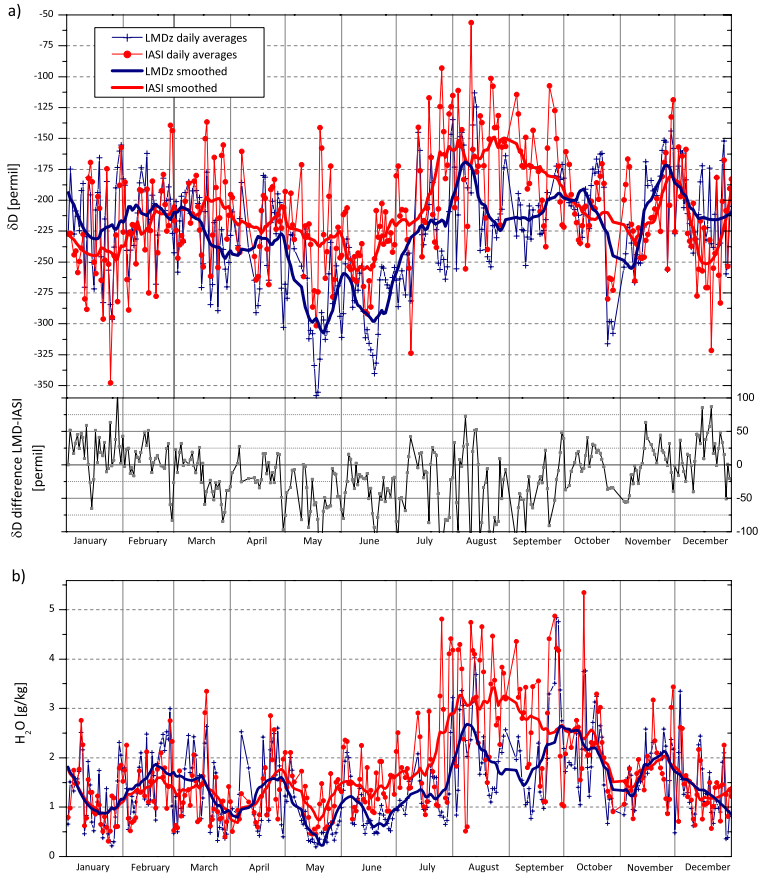

Fig. 7. Same as Fig. 6 but for the Izaña site.

ACPD
12, 13053–13087, 2012

Mid-tropospheric δD observations from IASI/MetOp

J.-L. Lacour et al.

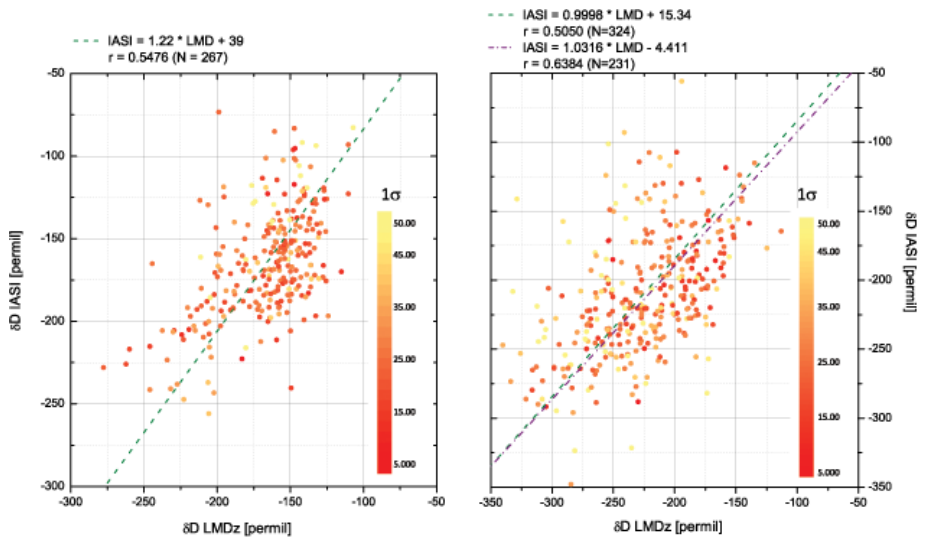

Fig. 8. Scatter plots of daily averaged δD IASI observations versus LMDz-iso simulations for Izaña site (right) and Darwin site (left). The color scale indicates the daily variability (1σ) of IASI retrieved values in the model grid box. The dashed and the dashed-dotted lines are reduced major axis regressions, on all points (dashed green lines) and, for Izaña, on points with a 1σ variability in the model grid box lower than 35. In the case of Izaña there is clear increase of the correlation coefficient (from 0.5 to 0.64) when considering only δD averages with a certain variability threshold (averages with a daily variability inferior to 35 ‰ (dashed-dotted violet line)). The line equations, the correlation coefficient and the number of coincident values are given above the figures.

ACPD
12, 13053–13087, 2012

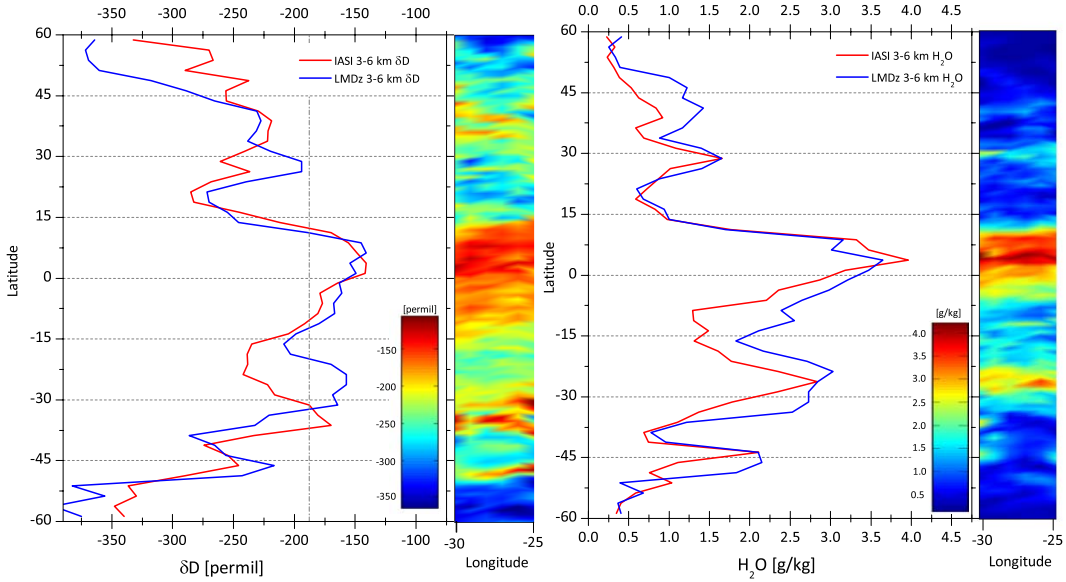

Fig. 9. Latitudinal distribution of δD (left) with δD a priori (gray dashed-dotted line) and H_2O (right) retrieved with IASI (red) and simulated by LMDz-iso (blue). δD retrievals, representative of the 3–6 km layer have been averaged on the first 15 days of January 2010 and on the LMDz-iso grid boxes. The corresponding spatial distributions of IASI retrievals are mapped besides the latitudinal gradients.

ACPD
12, 13053–13087, 2012